Multistate current-induced magnetization switching in Au/Fe/MgO(001) epitaxial heterostructures

P. Gospodarič,[1] E. Młyńczak,[1,2,*] I. Soldatov,[3,4] A. Kákay,[5] D. E. Bürgler,[1] L. Plucinski,[1] R. Schäfer,[3,6] J. Fassbender,[5] and C. M. Schneider[1,7]

[1]*Peter Grünberg Institut PGI, Forschungszentrum Jülich and JARA- Fundamentals of Future Information Technologies, 52425 Jülich, Germany*

[2]*Jerzy Haber Institute of Catalysis and Surface Chemistry, Polish Academy of Sciences, Niezapominajek 8, 30-239 Krakow, Poland*

[3]*Leibniz Institute for Solid State and Materials Research Dresden (IFW Dresden), Institute for Metallic Materials, 01069 Dresden, Germany*

[4]*Institute of Natural Sciences and Mathematics, Ural Federal University, 620083, Ekaterinburg, Russia*

[5]*HZDR, Institute of Ion Beam Physics and Materials Research, 01328 Dresden, Germany*

[6]*Institute for Materials Science, TU Dresden, 01062 Dresden, Germany*

[7]*Fakultät für Physik, Universität Duisburg-Essen, 47057 Duisburg, Germany*

(Received 23 December 2020; revised 17 March 2021; accepted 29 March 2021; published 3 May 2021)

Magnetization switching using in-plane charge current recently has been widely investigated in heavy metal/ferromagnet bilayers with the switching mechanism usually attributed to the action of the spin-orbit coupling. Here we study in-plane current induced magnetization switching in model epitaxial bilayers that consist of Au(001) and Fe(001) grown on MgO(001). We use the planar Hall effect combined with magnetooptical Kerr effect (MOKE) microscopy to investigate magnetic properties of the bilayers and current-induced switching. We show that a current density beyond 1.4×10^7 A/cm^2 can be employed for reproducible electrical switching of the magnetization between multiple stable states that correspond to different arrangements of magnetic domains with magnetization direction along one of the in-plane easy magnetization axes of the Fe(001) film. Lower current densities result in stable intermediate transversal resistances which are interpreted based on MOKE-microscopy investigations as resulting from the current-induced magnetic domain structure that is formed in the area of the Hall cross. We find that the physical mechanism of the current-induced magnetization switching of the Au/Fe/MgO(001) system at room temperature can be fully explained by the Oersted field, which is generated by the charge current flowing mostly through the Au layer.

DOI: 10.1103/PhysRevResearch.3.023089

I. INTRODUCTION

The possibility to manipulate magnetization orientation using electric current rather than magnetic field is indispensable in modern spintronics [1]. Spin transfer torque (STT) is now widely used in commercial STT-MRAM (magnetic random access memory) to switch the magnetization of a free layer in a magnetic tunnel junction (MTJ). In the last years, the prospects of even wider functionalities of MTJ have come into play with the discovery of a possibility of magnetization switching using in-plane charge current *via* spin-orbit torques (SOTs) [2–4]. Nowadays, the applications of spin-orbitronic devices not only to store but also to process information in the emerging fields of in-memory computing, probabilistic computing, and neuromorphic computing are envisioned [5].

The basic research that led to these practical SOT applications originated from the experiments on thin film bilayers consisting of a ferromagnet (FM) and a heavy metal (HM) layer [2,3], where an in-plane charge current affects the magnetization of the FM via the spin Hall effect [6] or inverse spin galvanic effect (iSGE, also known as the Rashba-Edelstein effect) [3,7]. In some of the subsequent works, the role of the heavy metal was overtaken by a layer of a topological insulator [8] or a transition metal dichalcogenide [9]. SOT effects have also found an exciting application as a means to manipulate the Néel vector of an antiferromagnetic layer speeding up the development of antiferromagnetic spintronics [10].

In this work, we are going back to basics by investigating in-plane current-induced switching of the magnetization of a prototypical ferromagnetic layer, Fe(001). We have grown epitaxial Fe(001) films on MgO(001) substrates and used an Au(001) overlayer to complete the epitaxial stack. Fe(001) films interfaced with MgO(001) have a rich history in spintronics research, forming the first epitaxial Fe/MgO/Fe trilayers that showed a giant tunneling magnetoresistance effect [11,12] and allowing the electric field control of the magnetic anisotropy in thin Fe(001) films deposited on MgO(001) [13]. A significant SOT effect has already been reported in single-crystalline Fe(001) films, but, to our knowledge, only for those deposited on GaAs(001) [14]. Moreover, in the epitaxial Fe/GaAs(001) systems the magnetization

*e.mlynczak@fz-juelich.de

switching by the Oersted field generated by an overlaying conductive wire separated from the Fe layer with an insulator was demonstrated [15]. The Fe/GaAs(001) system is much different from Fe/MgO(001) since the former is characterized by the interface of C_{2v} symmetry (twofold), while the latter is fourfold symmetric. SOT in heterostructures containing Fe/MgO interfaces have been to date reported in polycrystalline systems prepared by sputter deposition [16]. The potential advantages of the epitaxial systems are well-defined interfaces, which could enhance iSGE, and the existence of the magnetocrystalline anisotropy as the anisotropy fields present in a crystalline film may assist deterministic magnetization switching even in the absence of additional external magnetic fields.

We chose the Au(001)/Fe(001)/MgO(001) epitaxial system due to the good lattice match between the crystal structures of the three materials, and the Au/Fe stacking sequence was selected over the reversed one (Fe/Au), since an increased segregation of Au and Fe-Au intermixing has been observed in the latter at room temperature [17]. The Au/Fe bilayers were lithographically patterned into Hall bars, and the planar Hall effect (PHE) was used as a means to investigate the magnetization state in relation to the electrical current flowing along the Hall bar. PHE measurements are often used to demonstrate current-induced magnetization switching in FMs [15,16,18–20] and antiferromagnets [21]. We show that the magnetization of the Fe film reorients between two orthogonal easy axes when a longitudinal current density $j > 10^7$ A/cm^2 is applied along the Hall bar. A combination of transport measurements and Kerr microscopy revealed that a varying PHE transversal voltage is induced by the changes of the domain structure in the Hall cross, which can be controlled by the amplitude of the applied longitudinal current.

The studied Au/Fe/MgO(001) Hall bars exhibit a nonvolatile response to the applied current pulses which also depends on the history of the applied current density (i.e., amplitude of current that has been applied to the device). Interestingly, both the nonvolatility and the dependence on the past activity of the PHE-based Au/Fe(001) devices are characteristic for memristors, which are proposed as the building blocks for neuromorphic computing architectures [22].

II. EXPERIMENTAL METHODS

The MgO(001) single-crystal substrates were prepared in ultra-high vacuum conditions by annealing at 500 °C for 30 min, which resulted in a clear, background-free, low-energy electron diffraction (LEED) pattern. The Au/Fe bilayers of different thicknesses were prepared on MgO(001) substrate by molecular beam epitaxy at room temperature. Sharp LEED spots proved high crystalline quality of the films and confirmed the epitaxial relation: Au(001)[110]‖Fe(001)[100]‖MgO(001)[110]. The Fe layer thickness was optimized to find the balance between small enough magnetic anisotropy, which is preferential for current induced switching experiments, and continuity of the film providing well-defined fourfold magnetocrystalline anisotropy. Discussion of this procedure, based on the results of additional magnetic measurements, can be found in the Appendix Sec. A.1. The Au(4 nm)/Fe(1.5 nm) bilayers were chosen for further studies, and results obtained for these samples will be discussed in this article. We checked, by *ex situ* x-ray absorption spectroscopy, that 4 nm Au protects Fe film from oxidation in ambient conditions (Appendix Sec. A.2); therefore no additional cap layer was necessary. The Au/Fe(001) bilayers were photolithographically patterned into the Hall bar structures ($L = 700$ μm, $W = 18$ μm) as shown in Fig. 1(a). The Hall bars were designed to be oriented parallel to the Fe[110] direction, i.e., the hard magnetic axis of the in-plane magnetized Fe(001) film.

The planar Hall effect (PHE) measurements were performed in a magneto-transport setup in a cryostat kept at $T = 280$ K. The sample with the patterned Hall bars was electrically connected to a chip carrier using Al bonding wires. The chip carrier was placed in the sample stage located at the end of a rotatable rod connected to a stepper motor for automatic rotation of the sample. Each pin of the chip carrier was connected to a wire leading through the rod and a feedthrough to a DC current source or a voltage meter. The rod was placed between two water-cooled electromagnets, which generate a uniform magnetic field up to ∼2 T.

The Kerr microscopy images were acquired using a MOKE microscope. Before entering the microscope, light from eight LEDs is guided by glass fibers into a cross-like arrangement, which enables switching between different Kerr geometries and achieving *pure* in-plane magnetic contrast. The details of the setup are described in Ref. [23]. The sample mounted in the Kerr microscope is electrically connected to a DC current source and a multimeter, which allows for simultaneous transport and Kerr measurements.

III. EXPERIMENTAL RESULTS

A. Magnetic properties of the Au/Fe(001) Hall bars

The magnetic properties of the bilayers were investigated using the PHE, since the studied samples exhibit a strong in-plane magnetic anisotropy. The transversal PHE resistance $R_{xy} = V_{xy}/I$ was measured for different angles φ_B between the in-plane saturating magnetic field $\vec{B}_{\text{ext}} = 400$ mT and the applied longitudinal current $\vec{I}$, as shown in Fig. 1(a). Since this measurement was performed in saturation, the angle of the magnetization with respect to the long axis of the Hall bar (which is aligned to the Fe[110] direction), φ_M, strictly follows φ_B ($\varphi_M = \varphi_B$). The angular dependence of the PHE shows a nearly ideal $\sin(2\varphi_M)$ dependence [Fig. 1(b)], with small deviations that can be attributed to the imperfect experimental geometry. This result can be used to identify the magnetization direction φ_M from the R_{xy} measured in subsequent experiments. Specifically, we see that due to the chosen orientation of the Hall bar with respect to the crystalline directions of the sample, the maxima and minima of the planar Hall resistance are observed when the magnetization points along Fe[010], Fe[$\bar{1}$00], Fe[0$\bar{1}$0], and Fe[100] (φ_M= 45°, 225°, 135°, and 315°), while zero planar Hall voltage is measured when the magnetization is aligned with Fe[110], Fe[$\bar{1}$10], Fe[$\bar{1}\bar{1}$0], and Fe[1$\bar{1}$0] ($\varphi_M = 0°$, 90°, 180°, and 270°). Consequently, a switch of the magnetization between two orthogonal directions can be detected as a jump between

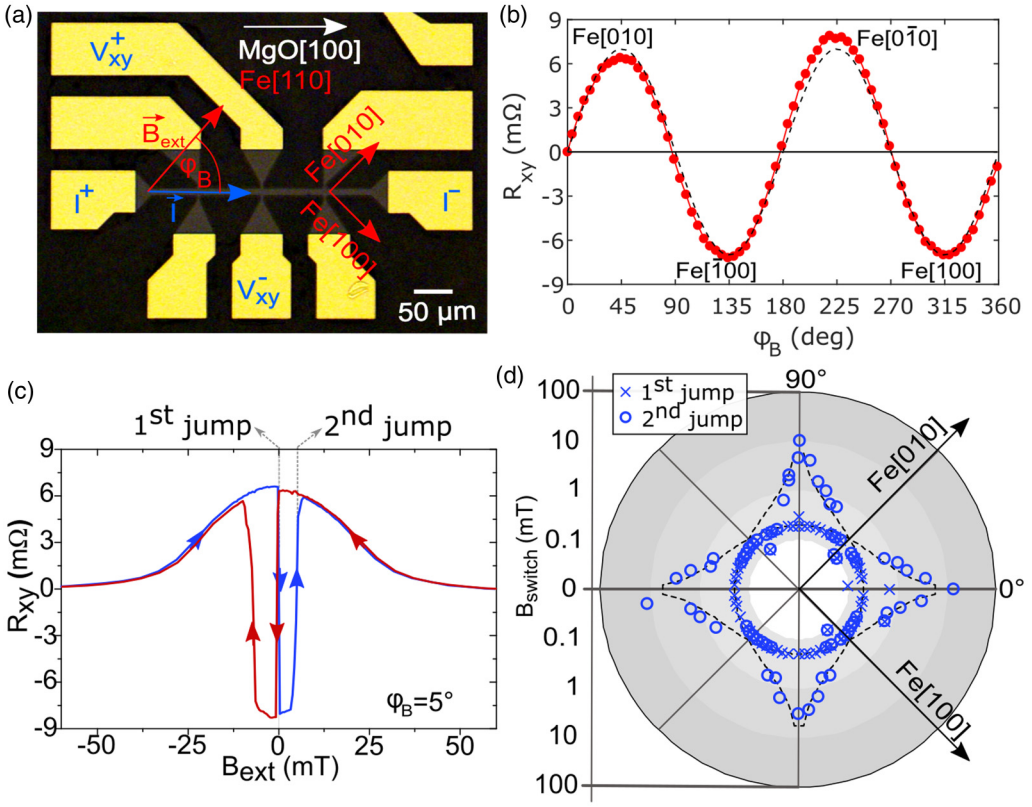

FIG. 1. Magnetic properties of the Au/Fe/MgO(001) Hall bars. (a) The Hall bar pattern with a sketch of the geometry for the magneto-transport measurements. (b) Planar Hall effect angular dependence. (c) Response of the transversal resistance R_{xy} to external magnetic field scanned between −60 and 60 mT and applied at an angle $\varphi_B = 5^\circ$ to the longitudinal current $\vec{I}$. (d) Angular plot of the magnetic fields B_{switch} of the first and second jump in R_{xy} derived from the positive B_{ext} scan of the planar Hall effect hysteresis loops. The cubic symmetry of the B_{switch} of the second magnetization jump reflects the fourfold magneto-crystalline anisotropy of the Fe(001) thin film.

a minimum and a neighboring maximum (or *vice versa*) of $R_{xy}(\varphi_M)$.

The magnetic hysteresis loop measured with the external magnetic field close to the Fe[110] direction, along $\varphi_B = 5^\circ$, is shown in Fig. 1(c). At the beginning of the cycle, when the negative $\vec{B}_{\text{ext}}$ ($\varphi_B = 185^\circ$) is sufficient to saturate the magnetization, the value of R_{xy} is close to zero. When $\vec{B}_{\text{ext}}$ approaches zero, R_{xy} gradually increases up to more than 6 mΩ [blue line in Fig. 1(c)], which indicates rotation of the magnetization vector towards Fe[0$\bar{1}$0]. Next, directly after crossing zero field ($\vec{B}_{\text{ext}} = 0.1$ mT), the resistance jumps to the negative value of approximately $R_{xy} = -7$ mΩ, which indicates magnetization switching towards Fe[100], followed by another one to Fe[010]. Finally, the magnetization rotates gradually towards $\varphi_M = 5^\circ$. In this case, the sequence of jumps in counterclockwise direction results from the direction of the external field. The hysteresis loops were measured for different values of φ_B, out of which we derive the values of B_{ext} of the first and second jumps during the positive magnetic field scan (B_{switch}), which are plotted in Fig. 1(d). While the magnetic field of the first jump remains in the order of 0.5 mT for all φ_B, the fields of the second jump reach values beyond 10 mT at $\varphi_B = 0^\circ$ and for each 90° rotation of B_{ext}. In these cases, the first jump is suppressed, and the magnetization reversal proceeds via a single jump along the principle axes of the Fe(001) film. These results reveal the fourfold magnetic anisotropy of our samples, with the magnetic easy axes along Fe[100] and Fe[010] directions, as expected for a high-quality epitaxial Fe(001) thin film on MgO(001). No indication of an additional uniaxial magnetic anisotropy was observed.

B. Current-driven hysteresis loop

To investigate the current-induced magnetization reorientation, we measured R_{xy} for increasing longitudinal current I. Prior to the experiment, the magnetization was saturated along the Fe[010] direction using a magnetic field $B_{\text{ext}} = 400$ mT. After saturation, a small reference magnetic field $B_{\text{ref}} \sim 1$ mT was applied parallel to the Fe[$\bar{1}$10] direction and kept constant throughout the experiment in order to stabilize the switching behavior and to prevent a 180° rotation of the magnetization. The longitudinal current with positive polarity was scanned from 1 mA up to 25 mA and back [black dots in Fig. 2(a)]. Identical values of the transversal resistance R_{xy} were obtained at the beginning and at the end of the current scan [state marked by a numeral 1 in Fig. 2(a)]. Apparently, in this case, the magnetization state of the sample remained constant, as the monotonic increase of the resistance proportional to $|j|^2$ should be attributed to Joule heating of the Hall bar. Immediately after the positive current scan, the polarity of the current was reversed and the scan was repeated [blue dots in Fig. 2(b)]. This time, a clear, current-induced magnetic

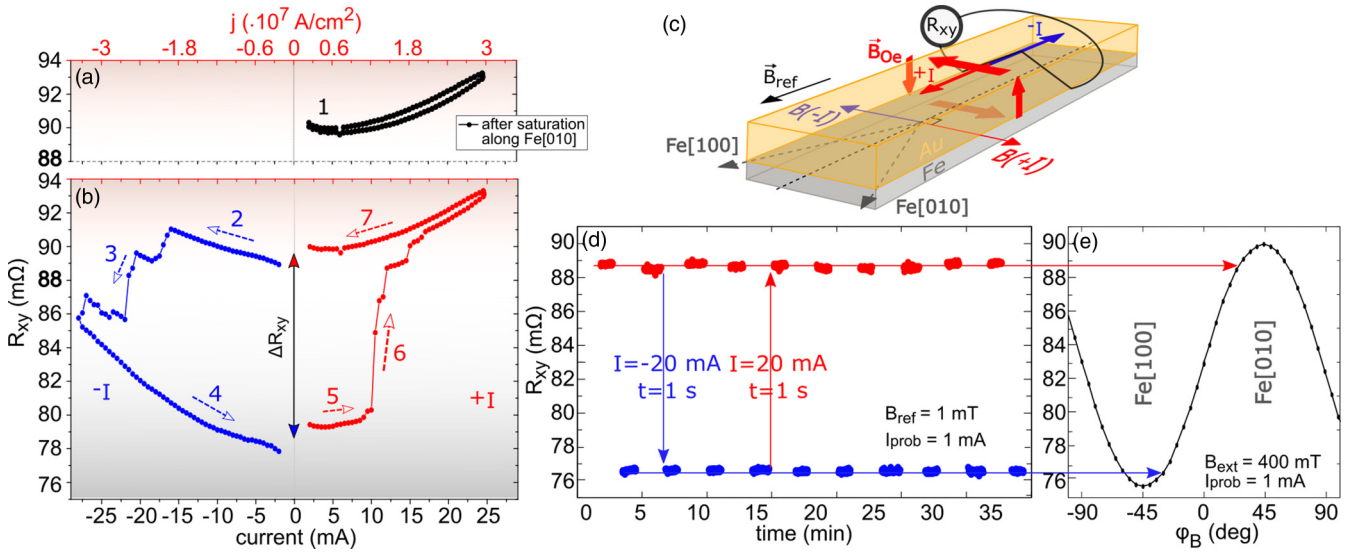

FIG. 2. Current-induced magnetization reorientation (a) Measurement of the PHE resistance R_{xy} with increasing longitudinal current I in Au/Fe(1.5 nm)/MgO(001) after saturation of the magnetization along the Fe[010] direction. (b) The numbers 1–7 mark the sequence of the measurements. First, a positive current $+I$ was scanned (1, black dots). Immediately afterwards, a negative current $-I$ was scanned (2–4, blue dots), followed directly by a positive current scan (5–7, red dots). A constant reference magnetic field B_{ref} ∼1 mT was applied in the Fe[$\bar{1}$10] direction in (a) and (b). (c) Sketch of the experiment. (d) The PHE resistance R_{xy} measured using a small probing current $I = 1$ mA (corresponding to $j = 1.2 \times 10^6$ A/cm^2) after applying "pulses" of $I = 20$ mA (corresponding to $j = 2.4 \times 10^7$ A/cm^2) of either positive (in red) or negative (in blue) polarity for ∼1 s to the Hall bar. A constant magnetic field B_{ref} ∼1 mT was applied along the Fe[$\bar{1}$10] direction. (e) The angular dependence of the PHE resistance R_{xy} measured with a probing current $I = 1$ mA and a saturating external magnetic field ($B_{\text{ext}} = 400$ mT).

hysteresis loop was observed. The magnetic state appears to reorient via several intermediate states [marked by a number 3 in Fig. 2(b)], which are seen as steps in the current-driven hysteresis loop for current densities beyond -1.8×10^7 A/cm^2. The intermediate magnetic states were observed also during the positive current scan (red dots), which was acquired directly after the negative current scan. The last segment of the positive scan reoriented the magnetization to its initial state.

Comparison of the R_{xy} values measured during the current scans to the measurement of the PHE angular dependence shown in Fig. 2(e) confirms that the magnetization reorients from Fe[010], set prior to the scan, towards Fe[100] when current densities $|j|>1.5\times10^7$ A/cm^2 of negative polarity are applied to the Hall bar. The opposite reorientation, namely, from angles close to Fe[100] towards Fe[010], is induced by high current densities of positive polarity. Additional current-induced magnetic hysteresis loops, measured using different speeds of the sweeping current, are presented in the Appendix B.

Next, we checked whether it is possible to switch the magnetization of our Au/Fe bilayers using a current pulse. We applied alternate "pulses" ($t \sim 1$ s) of high current ($I = 20$ mA) and negative/positive polarity along the Hall bar and measured the PHE resistance R_{xy} using a small DC probing current $I = 1$ mA after each high-current pulse [Fig. 2(d)]. The R_{xy} state induced by the positive current pulse is close to the value expected for the magnetization aligned with the Fe[010] direction, while the negative current pulse induced a R_{xy} value expected for the Fe[100] direction [Fig. 2(e)]. The observed magnetization switching between two orthogonal easy directions (Fe[010] and Fe[100]) is reversible and reproducible. Additional results of the current-induced switching, also using current densities below the threshold that provide the full switch, can be found in the Appendix B.

C. Multilevel current-induced switching

To investigate the origin of the intermediate R_{xy} states observed within the current-induced hysteresis [Fig. 2(b), region marked with the numeral 3], we performed an *in situ* magnetotransport experiment in a Kerr microscope. Pulses of increasing current $I = 19$ mA up to 27 mA were applied along the Hall bar for $t = 0.1$ s in the absence of the external magnetic field ($B_{\text{ext}} = 0$). After each pulse, a Kerr image was acquired and the transversal PHE voltage was measured using a probing current $I_{\text{prob}} = 1$ mA. The obtained results are presented in Fig. 3. The entire width of the Hall bar, together with the transversal contacts, can be easily identified within the field of view. In the initial magnetic state, which was set by the external magnetic field along the Fe[$\bar{1}$00] direction, most of the Hall bar appears bright, but in addition some narrow dark domains with domain walls perpendicular to the Hall bar can be seen [Fig. 3(a)]. We identify the dark domains as regions with the magnetization aligned to Fe[0$\bar{1}$0]. After each applied pulse of increased current, the dark domains were observed to increase in size and new ones were formed along the Hall bar [Figs. 3(b)–3(h)]. The PHE voltage V_{xy} was read out for each of the observed current-induced domain patterns and is plotted in Fig. 3(i). Comparing domain state in Figs. 3(b) and 3(c), taken after the first and forth pulse, respectively, one can notice that the dark domains considerably increase in size (compare the domain pattern within the orange

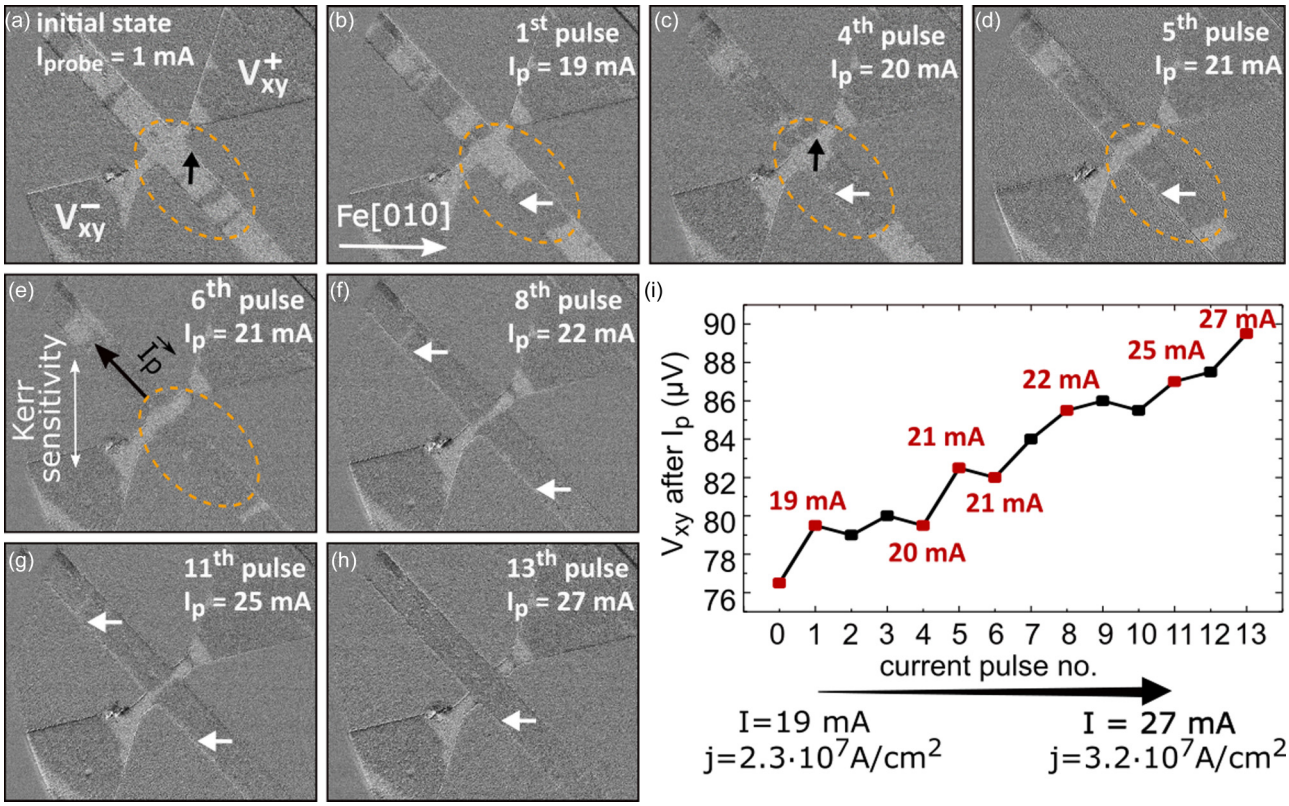

FIG. 3. The current-induced domain structure investigated by Kerr microscopy. A starting state of a homogeneous magnetization along the Hall bar saturated along the Fe[$\bar{1}$00] direction (bright domains) was set by applying a magnetic field. Afterwards, a sequence of Kerr images was acquired, each time after applying a 0.1-s-long current pulse along the Hall bar as marked in (e). Additionally, the PHE resistance of the induced magnetic state was measured using a 1 mA probing current between the contact pads marked in (a). (i) The transversal voltage V_{xy} values read out after each of the current pulses. The current of the applied pulses was increased in steps of 1 mA as indicated by the arrow below the graph. V_{xy} of the selected Kerr images (a–h) are marked in red.

ellipse). However, the simultaneously measured V_{xy} values remain approximately constant. Figure 3(d) shows the magnetic domain configuration after the pulse $I_p = 21$ mA, which has induced an increase of V_{xy} [Fig. 3(i)]. The dark magnetic domain within the orange ellipse has grown, and its borders are in the region of the Hall cross center. Small changes of the domain configuration within the Hall cross center are visible also between Figs. 3(e)–3(h), for which the corresponding V_{xy} gradually increases after the applied current pulses. We conclude that the measured PHE transversal voltage is mainly influenced by the magnetic state within the Hall cross center. Clearly, the switching between the Fe[$\bar{1}$00] [Fig. 3(a)] and Fe[0$\bar{1}$0] [Fig. 3(h)] directions proceeds *via* intermediate configurations of the magnetic domains with corresponding multiple transversal resistance R_{xy} states. This means that the current-induced intermediate states of the PHE voltage observed in the hysteresis loop [Fig. 2(b)] correspond to multidomain states within the Hall cross center.

D. Physical mechanism of magnetization switching

As briefly mentioned in the Introduction, in a HM/FM system, a few physical mechanisms of the current-induced magnetization switching can be expected. Since our samples are epitaxial Au/Fe bilayers characterized by strong magnetocrystalline anisotropy of the Fe layer as well as a well-defined interface, we will briefly mention here the possible switching mechanisms with the emphasis on the expectations for epitaxial systems.

The first mechanism to consider is the spin Hall effect (SHE), which describes generation of a spin current within the HM layer as a result of the charge current flow [6]. Microscopically, the sources of the SHE are the extrinsic mechanism of the spin-dependent scattering on the impurities [24] and an intrinsic mechanism that originates from the properties of the electronic band structure of the heavy metal layer [25,26]. Second, one can expect an inverse spin galvanic effect (iSGE), also referred to as Rashba-Edelstein effect, since the FM layer has broken inversion symmetry (the two interfaces are not equivalent; one of them is Au/Fe, the other is Fe/MgO). This effect originates from the spin-momentum locking of the electronic states within the interfacial region and is therefore sensitive to the details of the interfacial electronic structure [27,28]. The Rashba spin-orbit interaction introduces a nonequilibrium spin density, which acts on the magnetization *via* exchange coupling [27]. Both mentioned mechanisms depend on the spin-orbit interaction, and their effect on the magnetization is referred to as spin-orbit torques.

The current-induced torques act as additional field-like and damping-like terms in the Landau-Lifshitz-Gilbert equation, modifying the precessional magnetization dynamics [4]. The torques can always be rewritten in terms of the effective

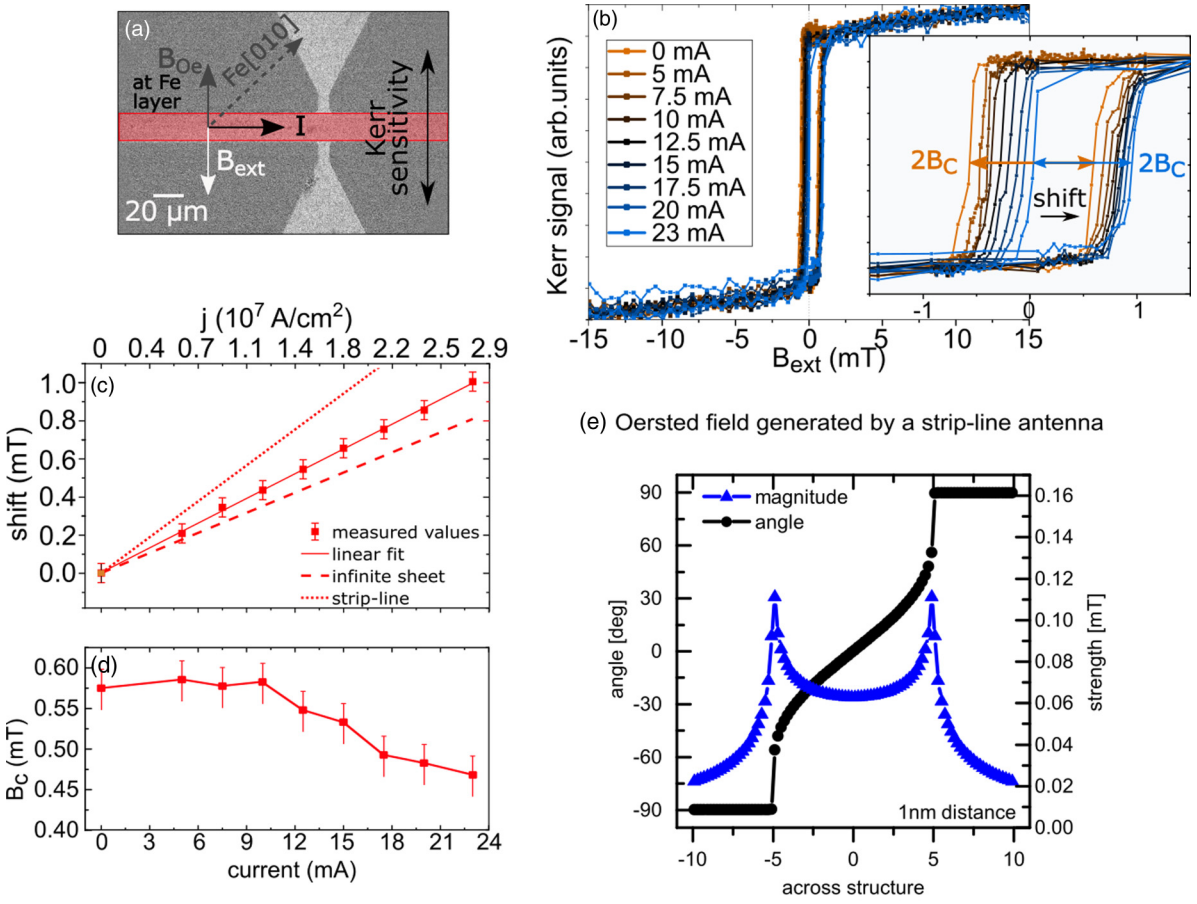

FIG. 4. (a) Kerr microscopy image of the Hall bar with current applied applied along Fe[110] and with external magnetic field $B_{\text{ext}} = 7$ mT along the Fe[1$\bar{1}$0] hard axis. The Kerr sensitivity was set parallel to the external magnetic field. The Kerr signal was extracted from the area marked in red. (b) The hard axis hysteresis loops were acquired for varying current density applied to the Hall bar. The inset shows the enlarged region of small magnetic fields where the shift (black arrow) of the hysteresis loops with respect to the zero external field and a decrease of the coercive field ($I = 0$ mA in orange and $I = 23$ mA in light blue) are visible for increasing current density. (c) Comparison of the experimentally observed hysteresis loop shift with the calculated values of the Oersted field for an infinite sheet (dashed line) and a strip line (dotted line). The current density was determined for the Hall bar width of 12 μm and total thickness of 5.5 nm. (d) The coercive field B_c was extracted from the width ΔB of the hysteresis loops as $B_c = \Delta B/2$. B_c stays constant for currents up to 10 mA and for higher currents begins to gradually decrease, which indicates the onset of increased sample heating. (e) Spatial variation of the magnitude and direction of the Oersted field calculated 1 nm above a strip-line antenna with a rectangular cross section carrying a current of 1 mA.

magnetic fields [4]. Then, for the current along the x axis, and z axis being the out-of-plane direction, one gets the field-like term $\vec{B_{FL}} = \tau_{FL} \cdot \hat{y}$, and a damping-like term $\vec{B_{DL}} = \tau_{DL} \cdot \vec{m} \times \hat{y}$. In our experiments, we can expect a field-like component of the current-induced field in the plane, perpendicular to the current flow, and the out-of-plane component of the damping-like field, due to the fact that in the steady state the magnetization lies in the sample plane. The SHE contributes mostly to the damping-like term, while iSGE has mainly a fieldlike effect on the magnetization [4]. Since Au is a HM characterized by a spin Hall angle (ratio of the generated spin current with respect to the charge current) that is relatively small, e.g., with respect to Pt [29], one should rather not expect a large SHE in the Au/Fe system; however, an iSGE needs not necessarily be small. Moreover, the fieldlike term tends to dominate in clean and well-ordered systems, in contrast to the damping-like term, which is more prominent in disordered ones [4].

In addition, we need to consider the classical effect of the current-induced magnetic field, i.e., the Oersted field, which is always generated by a current-carrying conductor. Since in our geometry Au is on top of the Fe layer, the Oersted field $\vec{B_{Oe}}$ generated by the current flowing predominantly through the Au layer will have the direction within the Fe layer and perpendicular to the current flow (along the y axis) [Fig. 2(c)], i.e., the same direction as a fieldlike term of SOT.

To investigate the physical mechanism of the observed current-induced magnetization reorientation in the Au/Fe(001) Hall bars we started from verifying whether any out-of-plane current-induced field $\vec{B_{DL}}$ is present in our system. We performed measurements of the $R_{xy}(\varphi_M)$ for increasing currents of both polarities (not shown). A $\vec{B_{DL}}$ component is expected to show up in $R_{xy}(\varphi_M)$ via the anomalous Hall effect contribution and should have a characteristic $\cos(\varphi_M)$ dependence, since the magnitude of the out-of-plane current-induced field $\vec{B_{DL}}$ depends on the angle between the magnetization and the current ($\vec{B_{DL}} = \tau_{DL} \cdot \vec{m} \times \hat{y}$), [16]. We did not observe any clear indications of a $\vec{B_{DL}}$ component during the room temperature measurements.

TABLE I. Room temperature cubic anisotropy constants K_4.

Thickness (nm)	K_4 (J/m^3)	Ref.
1.3	0.9×10^4	This work
1.5	1.5×10^4	This work
4.2	2.67×10^4	[33]
25	3.23×10^4	[35]
Bulk	4.8×10^4	[35]

Next, we considered the current-induced fields along the y direction, along which $\vec{B_{FL}}$ and the Oersted field are expected. To achieve that, we used Kerr microscopy to measure the hysteresis loops by sweeping the external magnetic field along the Fe[1$\bar{1}$0] hard axis (i.e., perpendicular to the Hall bar) while applying a constant current from $I = 0$ mA up to $I = 23$ mA longitudinal to the Hall bar [Figs. 4(a)–4(b)]. We observed shifts of the hysteresis loops, which scale linearly with the applied longitudinal current as ∼0.04 mT/mA [Fig. 4(c)]. The shift towards positive magnetic fields can be explained by an additional magnetic field in the Fe[$\bar{1}$10] direction, which is induced by the current.

To assess the magnitude of the Oersted field induced by the current flow, we made a simple calculation of the expected strength of the Oersted field in our experimental geometry. At first, we approximate the conductive bilayer with an infinite metallic sheet, because of the low ratio between the thickness t and width W of the Hall bars ($t/W \sim 1/4000$). The Oersted field generated by an infinite conducting sheet can be calculated as $B_{Oe} = \frac{\mu_0 i}{2}$ [30], where i stands for the current per unit transverse length. For $W = 18$ μm we find that the current-generated magnetic field is of the order of 0.035 mT/mA. We compare this result to the experimental data in Fig. 4(c), where the Oersted field expected assuming the infinite sheet model is shown by a dashed line. We see that the theoretical expectation is very close to the experimental value, yet the theory slightly underestimates the field magnitude.

To further investigate this issue, we performed another type of calculation, where we modeled our Hall bar as astrip-line antenna. The magnetic field of a strip-line antenna with a rectangular cross section was calculated by direct integration of the field produced by elementary currents. The details of the analytical model and the resulting formulas to compute the spatial dependent magnetic field outside of the antenna can be found in Ref. [31]. Since a much larger portion of the DC current applied to the Hall bar is expected to flow in the thicker and more conductive Au layer compared to the 1.5-nm-thick Fe film, in our model the antenna mimics the current-carrying Au layer, while the Fe layer is assumed to carry no current. In Fig. 4(e) we show the magnitude of the field 1 nm above the conductor (antenna) surface, i.e., within the Fe film. The generated Oersted field as a function of position along the width of the Fe magnetic layer (across the Hall-bar structure) is calculated for the current of 1 mA. As we can see, the magnitude reaches its maximum at the edge of the conductor. The angle shows that the field changes from a polar character at the edges to a transversal field in the middle of the sample. Depending on the polarity of the applied longitudinal current, the current-induced Oersted field $\vec{B}_{Oe}$ in the middle of the sample points along the Fe[$\bar{1}$10] or Fe[1$\bar{1}$0] direction in the present geometry of the Hall bar [see the schematics in Fig. 2(c)]. The magnitude of the in-plane field calculated in the middle of the strip-line antenna is then also plotted in Fig. 4(c) (dotted line). In this case, the theoretical prediction overestimates the magnitude of the shift with respect to the experiment. The reason for that is apparently the assumption that we used in the model, i.e., that the entire current flows through the Au layer. Knowing that, we can conclude that both models (infinite sheet and strip-line antenna) give results comparable to our experimental findings, and small discrepancies can be attributed to the assumptions of the models that do not ideally capture the geometry of the devices. This means that the current-induced in-plane magnetic field observed in our samples can be explained by the classical Oersted field, with no clear indication of the fieldlike component related to SOT. We note that a bilayer structure is essential for the observation of the Oersted-field-induced switching since the current flowing through a single magnetic layer generates an Oersted field that cancels out inside the film and thus cannot affect its magnetization state.

Moreover, in Fig. 4(d) we present B_c extracted from the full Hall bar, which starts to decrease at applied currents $I > 10$ mA [Fig. 4(d)], which indicates an increase of Joule heating. Hence, for increased current densities the Joule heating is not compensated by heat dissipation via contact pads and bonding wires and therefore increases the temperature of the Hall bar. The reduced B_c leads to a lower magnetic field required for switching of the magnetization between easy magnetization axes and can thus promote the onset of the switching process at lower applied current densities. While the Joule heating may assist the Oersted-field-driven magnetization reorientation, it cannot explain the reversibility and polarity-dependence of the observed magnetization switching mechanism [Fig. 2(d)].

Now, we can go back to the hysteresis loop measured with the external magnetic field applied at a small angle to the current direction (close to the Fe[110] direction) [Fig. 1(c)] to see how such small current-induced magnetic field (0.04 mT/mA) can induce a magnetization switching of the Fe(001) film. The PHE hysteresis loop in Fig. 1(c) shows that a magnetic field $B_{\text{ext}} > 5$ mT applied along a direction close to one of the hard magnetization axes is required to induce a 90° switch of the magnetization between the easy magnetization axes, within which $\vec{M}$ crosses the axis of B_{ext} (second jump of the PHE hysteresis loop). However, a magnetic field in the order of 0.5 mT along the hard axis suffices to induce the 90° jump, where $\vec{M}$ does not cross the B_{ext} axis (first jump of the PHE hysteresis loop). Therefore, a current-induced $\vec{B}_{Oe} < 1$ mT along the Fe[1$\bar{1}$0] hard axis can switch $\vec{M}$ either from Fe[010] to Fe[100] or *vice versa*, depending on the orientation of $\vec{B}_{Oe}$ as shown in Fig. 2.

IV. SUMMARY AND CONCLUSIONS

This paper presents experimental results of combined Kerr microscopy and magneto-transport measurements on epitaxial Au(4 nm)/Fe(1.5nm)/MgO(001) Hall bars. Our observations reveal that the magnetic state of Fe(001) layer can be ma-

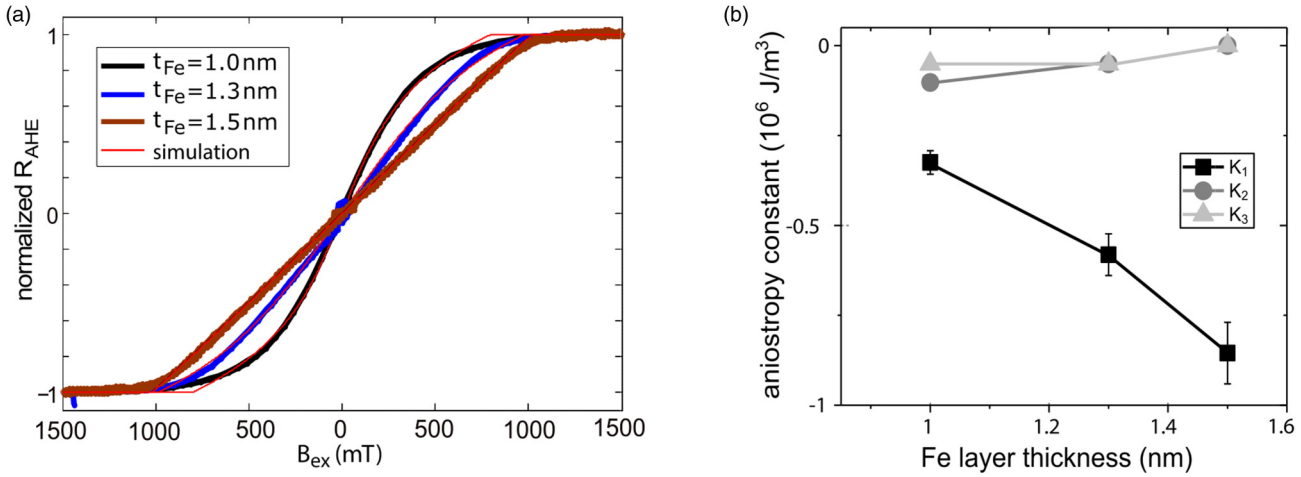

FIG. 5. (a) The results of the AHE measurements of Au/Fe/MgO(001) Hall bars of different Fe thicknesses. (b) The anisotropy constants derived from the AHE hysteresis loops.

nipulated by an applied longitudinal current, and we interpret the physical mechanism of switching as originating from the Oersted field. We did not observe any clear indications of spin-orbit torques for in-plane magnetized Au/Fe bilayers at the dimensions of our Hall bars and at room temperature. The Kerr microscopy shows formation of multidomain states, which can be distinguished in a transport measurement by the planar Hall voltage leading to multiple stable transversal resistance states. We demonstrated that the readout of the in-plane magnetic state in the Fe(001) layer *via* measurements of the planar Hall voltage locally probes the orientation of the magnetization at the Hall cross center. The PHE-based response of the devices to the applied current is nonvolatile and hysteretic, which makes the epitaxial Au/Fe(001) Hall bars an interesting system for further studies of current-induced switching and memristive behavior for neuromorphic computing. In this context, we note that our devices can be modified to the two-terminal geometry, where the anisotropic magnetoresistance rather than the planar Hall effect is used for sensing. Moreover, the discussed Fe(001) film can be switched with the magnetic field as small as 0.1 mT; therefore we expect that replacing Au in the discussed stack by another heavy metal such as Pt, or even a topological insulator, might lead to ultralow current-induced switching, when spin-orbit torque effects would truly come into play.

ACKNOWLEDGMENTS

We acknowledge fruitful discussions with F. Freimuth and Y. Mokrousov as well as the support of B. Beschoten and W. Skowronski in the initial stage of the project. Discussions with C. Schmitz are also acknowledged. This work was supported by the Initiative and Networking Fund of the Helmholtz Association and the statutory research funds of ICSC PAS within the subsidy of the Ministry of Science and Higher Education, Poland.

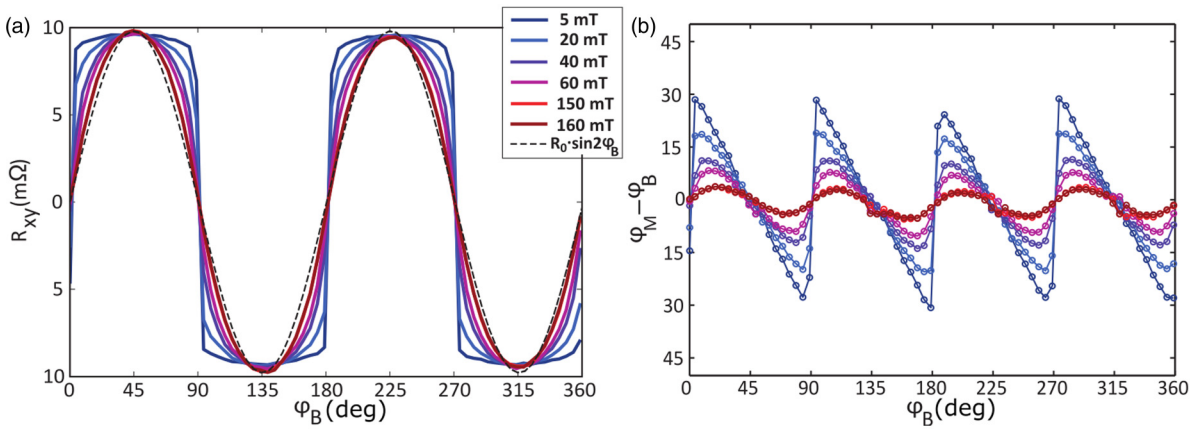

FIG. 6. (a) Result of an exemplary PHE measurement of the Au/Fe(1.3 nm)/MgO(001) Hall bar with different external magnetic fields from 5 to 160 mT compared to $R_0 \sin(2\varphi_B)$ with $R_0 = 9.6$ mΩ (broken line). These results were obtained at $T = 30$ K. The angle φ_B is measured between the applied current $I = 15$ mA and the direction of the external magnetic field. (b) The difference between the magnetization direction (φ_M) and the external magnetic field direction (φ_B) calculated for different magnetic fields from the deviation of the measured R_{xy} from the $R_{xy}(\varphi_B) \propto \sin(\varphi_M)\cos(\varphi_M)$ dependence expected at saturation.

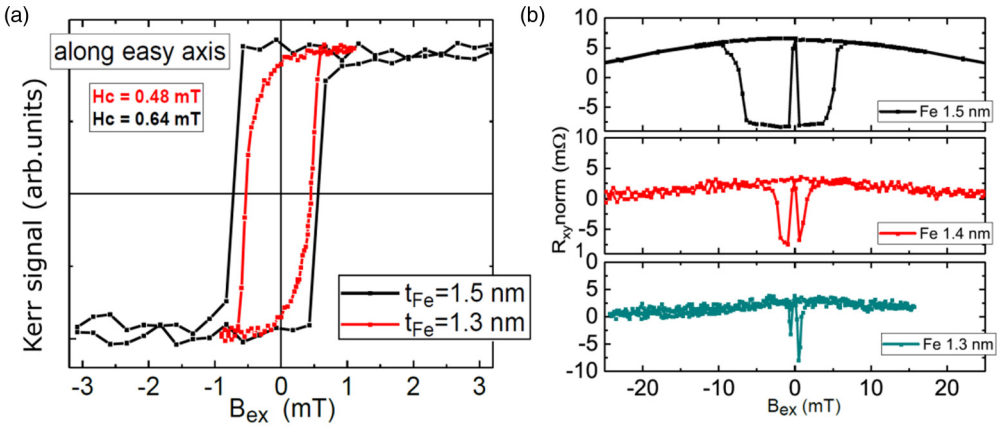

FIG. 7. (a) Results of the longitudinal MOKE measurements of the Au/Fe/MgO(001) Hall bars with different Fe thickness $t_{Fe} = 1.3$ nm and $t_{Fe} = 1.5$ nm along an easy magnetic axis. (b) Magnetic hysteresis measured using PHE in Au/Fe/MgO(001) Hall bars with different Fe thickness with magnetic field along a hard magnetic axis.

APPENDIX A: OPTIMIZATION OF THE LAYERS THICKNESSES

The Au/Fe/MgO(001) Hall bars that we discuss in the main part of the article have been optimized in terms of the Fe and Au thicknesses based on the results of the additional measurements that we will briefly discuss here.

1. Fe layer thickness

To achieve reproducible multistate current-induced switching we designed the Fe film to be thin enough to have relatively small magnetic anisotropy, and on the other hand, to be thick enough to be continuous in order to avoid the superparamagnetic behavior.

We analyzed the magnetic anisotropy in the Au/Fe/MgO(001) Hall bars of different Fe thicknesses. First, we derived anisotropy constants K_1 to K_3 that describe the out-of-plane anisotropy based on the anomalous Hall effect (AHE) measurements [Fig. 5(a)]. The anisotropy constants were determined by minimizing the Stoner-Wohlfarth equation:

$$\begin{aligned} E_m = & -M_S B_{ex} \cos(0^\circ - \Theta_M) \\ & - K_1 \cos^2(\Theta_M) \\ & - K_2 \cos^4(\Theta_M) \\ & - K_3 \cos^6(\Theta_M). \end{aligned} \tag{A1}$$

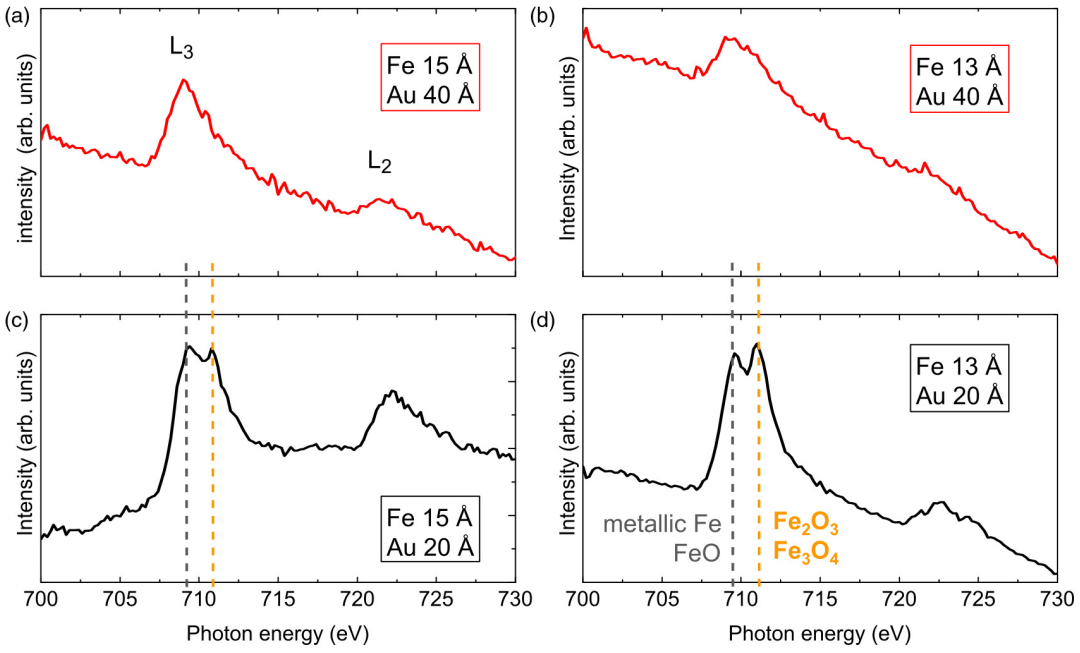

FIG. 8. Results of the XAS measurements of Au/Fe/MgO(001) Hall bars at the Fe $L_{2,3}$ absorption edge. The measurement was performed for two Fe thicknesses $t_{Fe} = 1.5$ nm and $t_{Fe} = 1.3$ nm and through Au capping layers 2 and 4 nm thick: (a) $t_{Fe} = 1.5$ nm and $t_{Au} = 4$ nm, (b) $t_{Fe} = 1.3$ nm and $t_{Au} = 4$ nm, (c) $t_{Fe} = 1.5$ nm and $t_{Au} = 2$ nm, (d) $t_{Fe} = 1.3$ nm and $t_{Au} = 2$ nm.

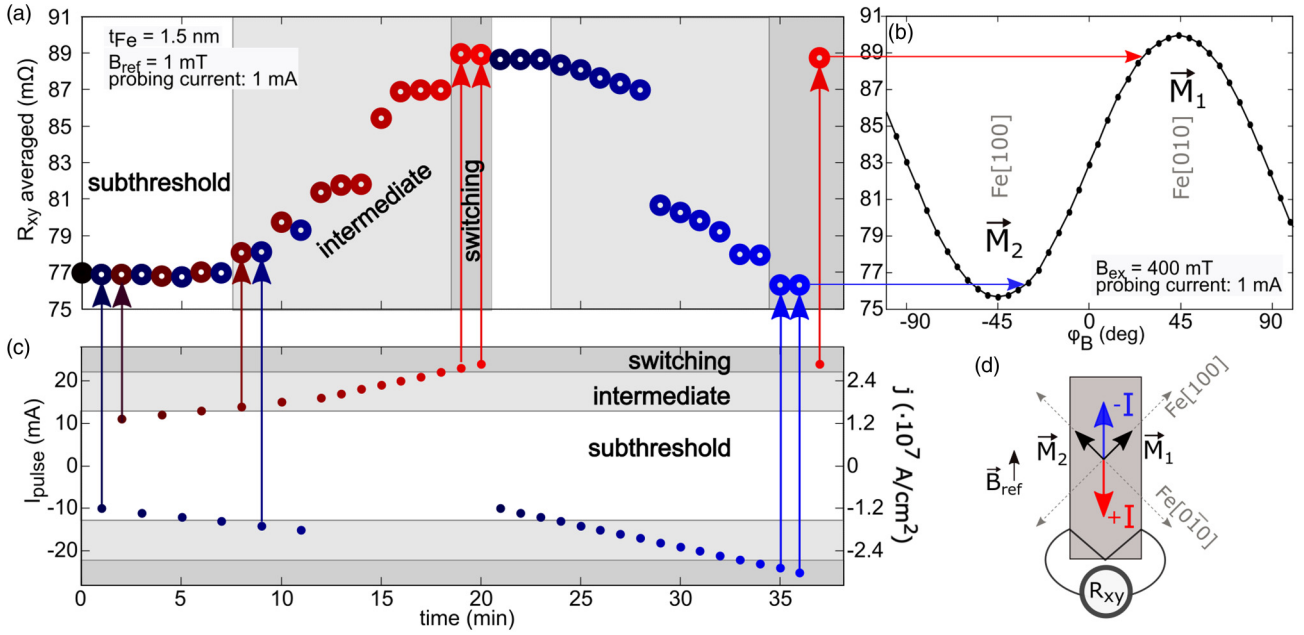

FIG. 9. Results of the current-induced magnetization switching experiment performed using Au (4 nm)/Fe(1.5 nm)/MgO(001) Hall bars. Different current ranges can be disgtinguished: (i) below the threshold for any switching (subthreshold), (ii) for intermediate switching into a magnetic domain state, and (iii) full switching into a saturated magnetization state. For details see the text.

The anisotropy terms up to the third order were included to obtain satisfactory fits to the measured data. The angle Θ_M is the angle between the normal and the magnetization, M_S stands for the saturation magnetization, and B_{ex} denotes the external magnetic field. The obtained values of the anisotropy constants K_1 to K_3 are negative, giving for small B_{ex} a minimum of E_m at $\Theta_M = 90$ °, i.e., in the sample plane. As shown in Fig. 5(b), this strong in-plane anisotropy is reduced when going towards thinner Fe films, which agrees with the expectations [32].

To determine the strength of the cubic anisotropy, we performed a magnetic torque analysis [33] based on the measurements of the planar Hall effect (PHE) below saturation. When the applied in-plane magnetic field B_{ex} is lower than the saturating field, the sample magnetization is tilted in the direction of B_{ex} and the magnitude of the tilt depends on the strength and direction of the magneto-crystalline and other in-plane anisotropy fields. An exemplary result of the PHE measured using different values of B_{ex} is presented in Fig. 6(a).

Figure 6(b) shows the deviation of the magnetization direction (φ_M) from the direction of the external magnetic field (φ_B), which is the largest for angles close to the hard magnetic axes ($\varphi_B = 0°$, 90°, 180°, and 270°) and smallest for angles close to the easy magnetic axes ($\varphi_B = 45°$, 135°, 225°, and 315°). We used the experimental ($\varphi_M - \varphi_B$) value as an input to derive the anisotropy constants acting in the sample plane based on the Stoner-Wohlfahrt model that contained not only the cubic but also uniaxial term. For the details of this procedure the reader is referred to Ref. [34]. We have found that the uniaxial term is negligibly small in our samples. The resulting values of the room temperature cubic anisotropy constant K_4 is reported in Table I. The temperature dependence of the cubic anisotropy constant K_4 is discussed in Ref. [34].

Additional magnetic measurements that we performed revealed that the samples with Fe thickness of $t_{Fe} = 1.3$ nm already show the signatures of discontinuity. This can be observed in longitudinal MOKE hysteresis loops [Fig. 7(a)], where the samples with $t_{Fe} = 1.3$ nm give loops of reduced squareness along an easy magnetization axis, which is a consequence of averaging over many interacting ferromagnetic islands. Magnetic hysteresis loops measured along a hard magnetic axis using PHE show dramatic differences between the samples of $t_{Fe} = 1.3$ nm, $t_{Fe} = 1.4$ nm, and $t_{Fe} = 1.5$ nm [Fig. 7(b)]. While the switching field of the first magnetization jump (switch to the closest easy axis) is very similar in each case, the switching field of the second jump (rotation towards a hard magnetic axis) increases by a factor of 10 between $t_{Fe} = 1.3$ nm and $t_{Fe} = 1.5$ nm. This behavior is related to the increase of the magnetic anisotropy of thicker films due to the improved continuity of the films.

We conclude that the Hall bars that contain Fe films with $t_{Fe} = 1.5$ nm are optimal for the current-induced magnetization switching. Results of these experiments are described in the main part of the article.

2. Au layer thickness

We designed the Au layer to be thick enough to assure a complete coverage of the Fe film. This served two purposes: (1) the formed structure was closer to an ideal bilayer as compared to the situation when the Au film would be discontinuous, and (2) the continuous Au film formed a protective layer for the Fe film to prevent its oxidation. To optimize the thickness of the Au layer, we performed additional measurements of the x-ray absorption spectroscopy (XAS). The measurements were performed at the beamline UE56-1 SGM of the storage ring BESSY II in Berlin. The XAS results for

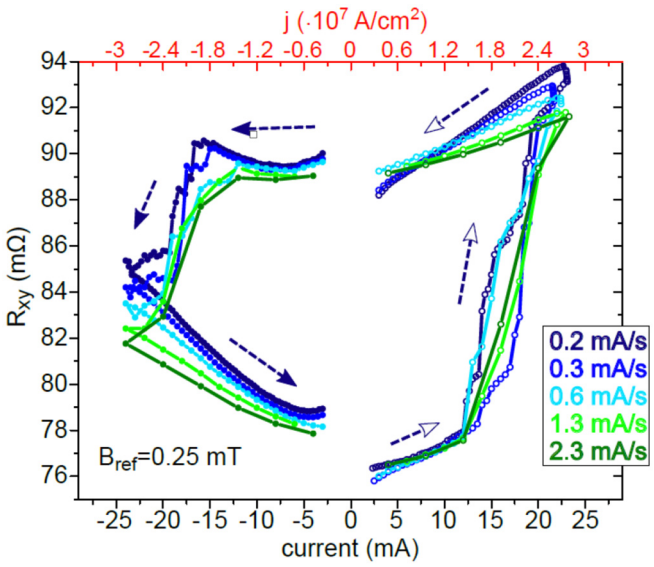

FIG. 10. Current-induced magnetic hysteresis loops measured using different speeds of the current sweep.

different layer thicknesses are presented in Fig. 8. We have analyzed the signal from the Fe $L_{2,3}$ absorption edge as seen through the Au top layer. The results for the 4-nm-thick Au layer show two peaks characteristic for metallic Fe [Figs. 8(a) and 8(b)]. We found that reduction of the Au thickness to 2 nm [Figs. 8(c) and 8(d)] results in the appearance of an additional peak that can be identified as originating from oxidized Fe [marked by a dashed yellow line in Figs. 8(c) and 8(d)]. We conclude that 4 nm of Au forms a protective film on top of Fe that prevents its oxidation; therefore for the subsequent experiments of the current-induced magnetization switching, we chose the samples with an Au thickness of 4 nm.

APPENDIX B: ADDITIONAL RESULTS OF THE CURRENT-INDUCED MAGNETIZATION SWITCHING

In this section we will present some of the additional results of the current-induced magnetization switching in Au (4 nm)/Fe(1.5 nm)/MgO(001) Hall bars.

In Fig. 9 results of an exemplary switching experiment are shown. Subsequent current pulses of varying amplitude and different polarities were applied to the device step by step [amplitude and polarity of each pulse is marked in Fig. 9(c)], and the transversal resistance was measured after each current pulse using small current density of 1.2×10^6 A/cm^2 [Fig. 9(a)]. The measured resistances can be translated to the magnetization direction using the PHE dependence $R_{xy}(\varphi_B)$ [Fig. 9(b)]. During this experiment, a small reference magnetic field of $B_{\mathrm{ref}} = 1$ mT was applied to the device [sketch in Fig. 9(d)]. At the beginning of the experiment, small current pulses are used and the transversal resistance does not change. This is the regime that we refer to as "subthreshold." Next, the current pulses are increased above 1.5×10^7 A/cm^2 resulting in the change of the magnetic state, as indicated by stable intermediate resistance values that gradually increase when the applied current density is increased (intermediate regime). When the current density is increased above 2.5×10^7 A/cm^2, the measured R_{xy} values correspond to the magnetization direction close to easy magnetization axes (full switching regime).

A set of the current-induced magnetic hysteresis loops measured with different current sweeping rates is shown in Fig. 10. In this experiment, the transversal resistance is measured during application of higher currents. The current was swept starting from zero towards positive current values and back, and subsequently towards negative current values, as shown by arrows in Fig. 10. The differences between the measured loops can be attributed to Joule heating. The increase of the temperature changes the resistivity of the conducting layer but also may affect formation of the magnetic domain structure responsible for the occurrence of the stable intermediate resistance states as explained in Sec. III C.

[1] A. Brataas, A. D. Kent, and H. Ohno, Current-induced torques in magnetic materials, Nat. Mater. **11**, 372 (2012).
[2] K. Ando, S. Takahashi, K. Harii, K. Sasage, J. Ieda, S. Maekawa, and E. Saitoh, Electric Manipulation of Spin Relaxation Using the Spin Hall Effect, Phys. Rev. Lett. **101**, 036601 (2008).
[3] I. M. Miron, G. Gaudin, S. Auffret, B. Rodmacq, A. Schuhl, S. Pizzini, J. Vogel, and P. Gambardella, Current-driven spin torque induced by the Rashba effect in a ferromagnetic metal layer, Nat. Mater. **9**, 230 (2010).
[4] A. Manchon, J. Železný, I. M. Miron, T. Jungwirth, J. Sinova, A. Thiaville, K. Garello, and P. Gambardella, Current-induced spin-orbit torques in ferromagnetic and antiferromagnetic systems, Rev. Mod. Phys. **91**, 035004 (2019).
[5] Y. Cao, G. Xing, H. Lin, N. Zhang, H. Zheng, and K. Wang, Prospect of spin-orbitronic devices and their applications, iScience **23**, 101614 (2020).
[6] J. E. Hirsch, Spin Hall Effect, Phys. Rev. Lett. **83**, 1834 (1999).
[7] A. Yu. Silov, P. A. Blajnov, J. H. Wolter, R. Hey, K. H. Ploog, and N. S. Averkiev, Current-induced spin polarization at a single heterojunction, Appl. Phys. Lett. **85**, 5929 (2004).
[8] A. R. Mellnik, J. S. Lee, A. Richardella, J. L. Grab, P. J. Mintun, M. H. Fischer, A. Vaezi, A. Manchon, E.-A. Kim, N. Samarth, and D. C. Ralph, Spin-transfer torque generated by a topological insulator, Nature (London) **511**, 449 (2014).
[9] Q. Shao, G. Yu, Y.-W. Lan, Y. Shi, M.-Y. Li, C. Zheng, X. Zhu, L.-J. Li, P. K. Amiri, and K. L. Wang, Strong Rashba-Edelstein effect-induced spinorbit torques in monolayer transition metal dichalcogenide/ferromagnet bilayers, Nano Lett. **16**, 7514 (2016).
[10] T. Jungwirth, X. Marti, P. Wadley, and J. Wunderlich, Antiferromagnetic spintronics, Nat. Nanotechnol. **11**, 231 (2016).
[11] S. Yuasa, T. Nagahama, A. Fukushima, Y. Suzuki, and K. Ando, Giant room-temperature magnetoresistance in single-crystal Fe/MgO/Fe magnetic tunnel junctions, Nat. Mat. **3**, 868 (2004).

[12] S. S. P. Parkin, C. Kaiser, A. Panchula, P. M. Rice, B. Hughes, M. Samant, and S.-H. Yang, Giant tunneling magnetoresistance at room temperature with MgO(001) tunnel barriers, Nat. Mater. **3**, 862 (2004).

[13] T. Maruyama, Y. Shiota, T. Nozaki, K. Ohta, N. Toda, M. Mizuguchi, A. A. Tulapurkar, T. Shinjo, M. Shiraishi, S. Mizukami *et al.*, Large voltage-induced magnetic anisotropy change in a few atomic layers of iron, Nat. Nanotechnol. **4**, 158 (2009).

[14] L. Chen, M. Decker, M. Kronseder, R. Islinger, M. Gmitra, D. Schuh, D. Bougeard, J. Fabian, D. Weiss, and C. H. Back, Robust spin-orbit torque and spin-galvanic effect at the Fe/GaAs (001) interface at room temperature, Nat. Commun. **7**, 13802 (2016).

[15] T. Yoo, S. Khym, H. Lee, S. Lee, S. Lee, X. Liu, J. K. Furdyna, D. U. Lee, and E. K. Kim, Quaternary memory device fabricated from a single layer Fe film, J. Appl. Phys. **111**, 07C704 (2012).

[16] M. Kawaguchi, K. Shimamura, S. Fukami, F. Matsukura, H. Ohno, T. Moriyama, D. Chiba, and T. Ono, Current-induced effective fields detected by magnetotrasport measurements, Appl. Phys. Express **6**, 113002 (2013).

[17] P. Gospodarič, E. Młyńczak, M. Eschbach, M. Gehlmann, G. Zamborlini, V. Feyer, L. Plucinski, and C. M. Schneider, Localized segregation of gold in ultrathin Fe films on Au(001), Phys. Rev. B **97**, 085409 (2018).

[18] T. Yoo, S. Khym, H. Lee, S. Lee, S. Kim, J. Shin, S. Lee, X. Liu, and J. K. Furdyna, Use of the asymmetric planar Hall resistance of an Fe film for possible multi-value memory device applications. J. Nanosci. Nanotechnol. **11**, 5990 (2011).

[19] X. Fan, J. Wu, Y. Chen, M. J. Jerry, H. Zhang, and J. Q. Xiao, Observation of the nonlocal spin-orbital effective field, Nat. Commun. **4**, 1799 (2013).

[20] M. Jamali, Z. Zhao, D. C. Mahendra, D. Zhang, H. Li, A. K. Smith, and J.-P. Wang, Planar Hall effect based characterization of spin orbital torques in Ta/CoFeB/MgO structures, J. Appl. Phys. **119**, 133902 (2016).

[21] P. Wadley, B. Howells, J. Železný, C. Andrews, V. Hills, R. P. Campion, V. Novák, K. Olejník, F. Maccherozzi, S. S. Dhesi *et al.*, Spintronics: Electrical switching of an antiferromagnet, Science **351**, 587 (2016).

[22] J. Grollier, D. Querlioz, and M. D. Stiles, Spintronic nanodevices for bioinspired computing, Proc. IEEE **104**, 2024 (2016).

[23] I. V. Soldatov and R. Schäfer, Selective sensitivity in Kerr microscopy, Rev. Sci. Instrum. **88**, 073701 (2017).

[24] R. V. Shchelushkin and Arne Brataas, Spin hall effects in diffusive normal metals, Phys. Rev. B **71**, 045123 (2005).

[25] J. Sinova, D. Culcer, Q. Niu, N. A. Sinitsyn, T. Jungwirth, and A. H. MacDonald, Universal Intrinsic Spin Hall Effect, Phys. Rev. Lett. **92**, 126603 (2004).

[26] G. Y. Guo, S. Murakami, T.-W. Chen, and N. Nagaosa, Intrinsic Spin Hall Effect in Platinum: First-Principles Calculations, Phys. Rev. Lett. **100**, 096401 (2008).

[27] A. Manchon and S. Zhang, Theory of spin torque due to spin-orbit coupling, Phys. Rev. B **79**, 094422 (2009).

[28] P. M. Haney, H.-W. Lee, K.-J. Lee, A. Manchon, and M. D. Stiles, Current-induced torques and interfacial spin-orbit coupling, Phys. Rev. B **88**, 214417 (2013).

[29] M. Isasa, E. Villamor, L. E. Hueso, M. Gradhand, and F. Casanova, Temperature dependence of spin diffusion length and spin Hall angle in Au and Pt, Phys. Rev. B **91**, 024402 (2015).

[30] N. Gauthier, Magnetic field of an infinite current-carrying ribbon, Am. J. Phys. **56**, 819 (1988).

[31] D. Chumakov, High frequency behaviour of magnetic thin film elements for microelectronics, Ph.D. thesis, Technische Universität Dresden, 2006.

[32] A. Kozioł-Rachwał, W. Skowroński, T. Ślezak, D. Wilgocka-Ślezak, J. Przewoźnik, T. Stobiecki, Q. H. Qin, S. van Dijken, and J. Korecki, Room-temperature perpendicular magnetic anisotropy of MgO/Fe/MgO ultrathin films, J. Appl. Phys. **114**, 224307 (2013).

[33] B. Hu, W. He, J. Ye, J. Tang, Y.-S. Zhang, S. S. Ahmad, X.-Q. Zhang, and Z.-H. Cheng, Determination of magnetic anisotropy constants and domain wall pinning energy of Fe/MgO(001) ultrathin film by anisotropic magnetoresistance, Sci. Rep. **5**, 14114 (2015).

[34] P. Gospodarič, Current-induced magnetization switching in a model epitaxial Fe/Au bilayer, Ph.D. thesis, University Duisburg Essen, 2019.

[35] S. Mallik, N. Chowdhury, and S. Bedanta, Interplay of uniaxial and cubic anisotropy in epitaxial Fe thin films on MgO (001) substrate, AIP Adv. **4**, 097118 (2014).